

Supporting Information

Chemistry of a series of heterobimetallic complexes $\text{Mn}^{\text{III}}_2(\text{Ca}^{\text{II}}/\text{Sr}^{\text{II}})\text{X}_2$ ($\text{X} = \text{Cl}^-$, Br^-)

Priyabrata Bhattacharya,^a Riya Bag,^a Ray J. Butcher,^b Snehanjali Behera,^c Biswajit Mondal^{c*} and Sanchita Goswami^{a*}

^aDepartment of Chemistry, University of Calcutta, 92, A.P.C. Road, Kolkata-700009, India.

^bChemistry Department, Howard University, Washington, D.C. 20059, United States.

^cDiscipline of Chemistry, IIT Gandhinagar, Palaj, Gujarat - 382055, India.

CONTENTS	Page No.
Figure S1. FT-IR spectrum of complexes 1 , 2 , 3 and 4 .	S4
Figure S2. PXRD of complexes 1 , 2 , 3 and 4 .	S5
Figure S3. ESI-MS spectrum of complex 1 in methanol.	S6
Figure S4. ESI-MS spectrum of complex 2 in methanol.	S7
Figure S5. ESI-MS spectrum of complex 3 in methanol.	S8
Figure S6. ESI-MS spectrum of complex 4 in methanol.	S9
Figure S7. UV-Visible absorption spectra of complexes 1 , 2 , 3 , 4 and H₂Vab .	S10
Figure S8. Crystal structure of complex 2 showing the trinuclear hetero-bimetallic core. Hydrogen atoms attached to carbon are removed for clarity. Color code: C = grey; N = blue; O = red; H = black; Cl = green; Mn ^{III} = purple; Sr ^{II} = gold.	S11
Figure S9. Crystal structure of complex 3 showing the trinuclear hetero-bimetallic core. Hydrogen atoms attached to carbon are removed for clarity. Color code: C = grey; N = blue; O = red; H = black; Br = brown; Mn ^{III} = purple; Ca ^{II} = yellow.	S11
Figure S10. Crystal structure of complex 4 showing the trinuclear hetero-bimetallic core. Hydrogen atoms attached to carbon are removed for clarity. Color code: C = grey; N = blue; O = red; H = black; Br = brown; Mn ^{III} = purple; Sr ^{II} = gold.	S12
Figure S11. A supramolecular 2D structure of complex 1 formed by $\pi \cdots \pi$ interactions between 1D sheets along the <i>b</i> axis which are formed by O-H \cdots O bonds along the <i>a</i>	S12

axis.

Figure S12. Molar magnetization (M) vs. magnetic field (H) for complexes 1-4 at 2.0 K	S13
Figure S13. Molar magnetization (M) vs. H/T plot for complexes 1-4 at 2.0 K.	S14
Figure S14. Temperature dependence of χ_M^{-1} for complexes 1-4 .	S15
Figure S15. CV data for complex 2 (red) and its metal-free analog (black) in DMF. 3 mm glassy carbon as working, Ag/AgCl as a reference, Pt wire as a counter electrode.	S16
Figure S16. Comparative time-dependent UV-Visible spectra for complex 2 : a) after the addition of water and b) after the addition of OH ⁻ .	S16
Figure S17. CV data for DMF with 200 mM OH ⁻ with (red) and without the catalyst (complex 2) (green) and only DMF (black dash). 3 mm glassy carbon as working, Ag/AgCl as a reference, Pt wire as a counter electrode.	S17
Figure S18. Gas chromatography (GC) Trace with complex 2 . a. Time-dependent GC trace for H ₂ O; b. OH ⁻ oxidation. High surface area graphite rod as working, Ag/AgCl as a reference, Pt wire as a counter electrode.	S17
Figure S19. OCP measurement in DMF. a. OCP measurement with 1000 mM H ₂ O; b. with 200 mM OH ⁻ . Pt as working, Ag/AgCl as a reference, Pt wire as a counter electrode. The reference is corrected with respect to the Fe ^{+/-} .	S18
Figure S20. a. Comparative CV for complex 2 , free ligand and blank carbon cloth in 1M KOH. b. time-dependent GC trace for OH ⁻ oxidation; c. Comparative CV for complex 2 , free ligand, and blank carbon cloth in pH 7 buffer.	S18
Table S1. Crystal refinement parameters of complexes 1-4 .	S19
Table S2. Selected bond lengths (Å) and bond angles (°) in complex 1 .	S20
Table S3. Selected bond lengths (Å) and bond angles (°) in complex 2 .	S22
Table S4. Selected bond lengths (Å) and bond angles (°) in complex 3 .	S24
Table S5. Selected bond lengths (Å) and bond angles (°) in complex 4 .	S26
Table S6. Bond Valence Sum (BVS) results for manganese centers in complex 1 in different oxidation states and their assignment.	S28
Table S7. Bond Valence Sum (BVS) results for manganese centers in complex 2 in different oxidation states and their assignment.	S28
Table S8. Bond Valence Sum (BVS) results for manganese centers in complex 3 in different oxidation states and their assignment.	S28

Table S9. Bond Valence Sum (BVS) results for manganese centers in complex 4 in different oxidation states and their assignment.	S28
Table S10. Continuous Shape Measures (CShMs) of manganese centers in complexes 1, 2, 3 and 4 respectively relative to ideal 5/6–vertex polyhedral. The lowest CShMs value which corresponds to closest geometry is highlighted.	S29
Table S11. Continuous Shape Measures (CShMs) of calcium and strontium centers in complexes 1, 3 and 2, 4 respectively relative to ideal 8–vertex polyhedral. The lowest CShMs value which corresponds to closest geometry is highlighted.	S30
Table S12. Hydrogen bond parameters found in complex 1 , (distances (Å), angles, (°)).	S32
Table S13. Hydrogen bond parameters found in complex 2 , (distances (Å), angles, (°)).	S32
Table S14. Hydrogen bond parameters found in complex 3 , (distances (Å), angles, (°)).	S32
Table S15. Hydrogen bond parameters found in complex 4 , (distances (Å), angles, (°)).	S32
Table S16. Electrochemical parameters for manganese complexes used in this study.	S33
Table S17. Over potential values of different complexes based on the OCP values.	S33
Table S18. OER half-wave potential of complexes with respect to NHE.	S34

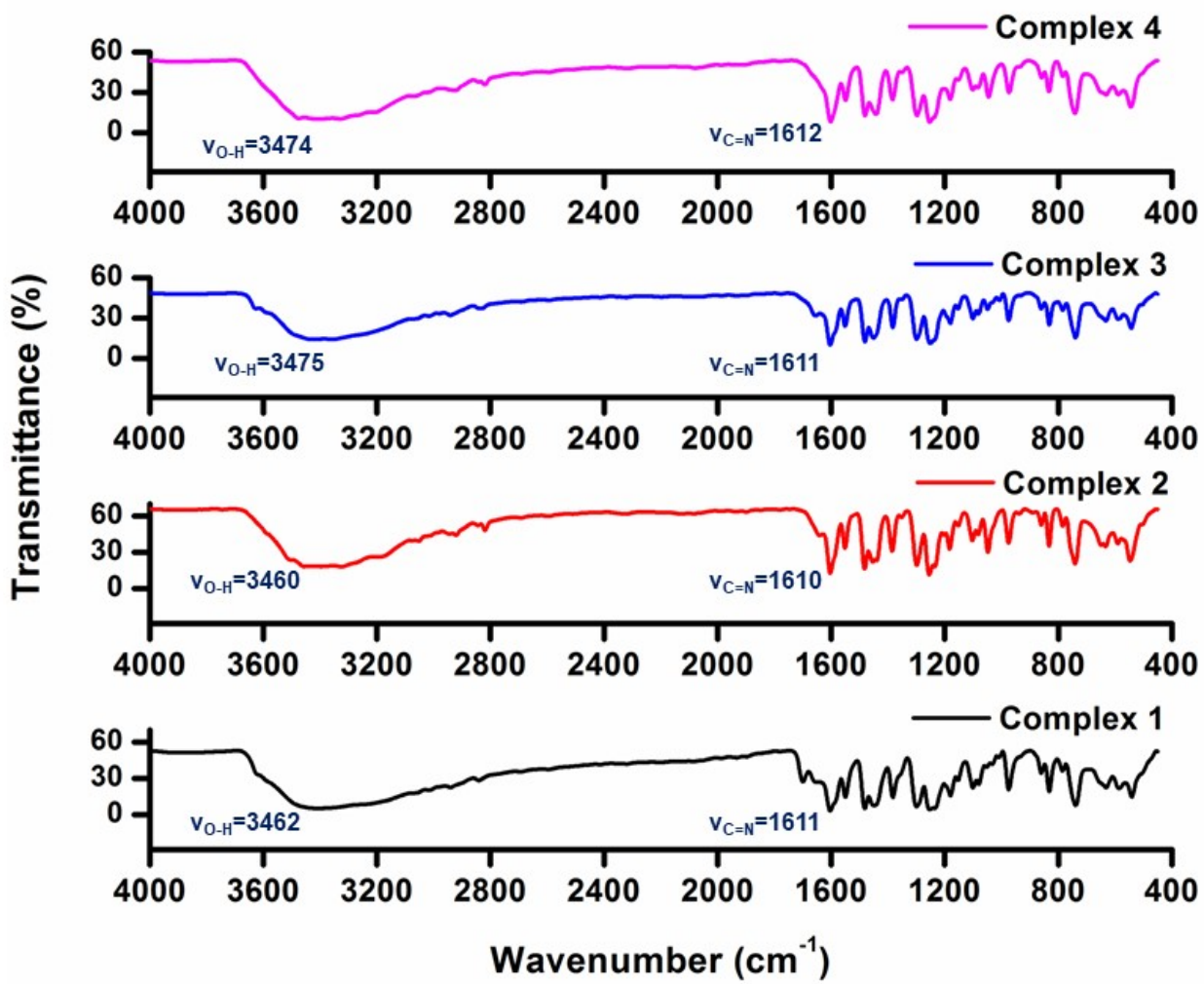


Figure S1. FT-IR spectrum of complexes 1, 2, 3 and 4.

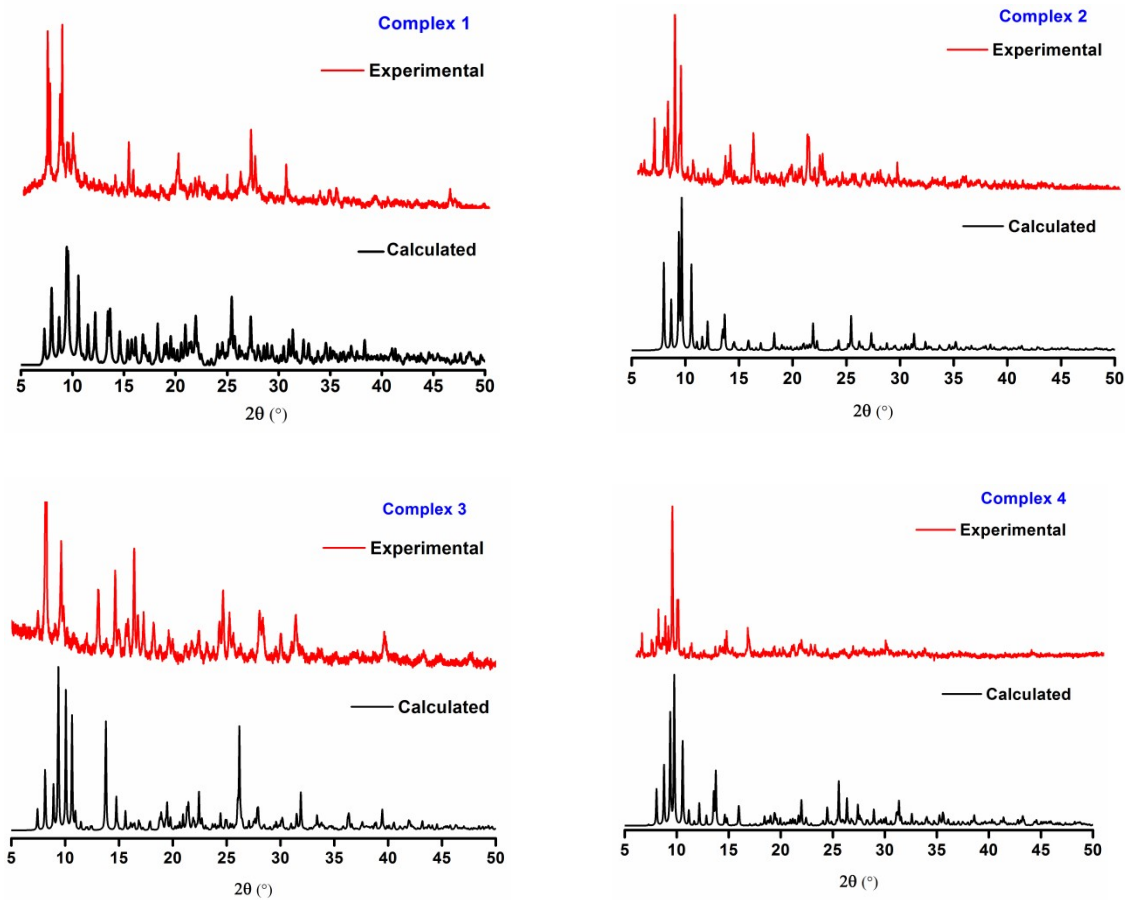


Figure S2. Experimental (red) and calculated (black) Powder X–ray diffraction spectrum of complexes **1**, **2**, **3** and **4** to determine the phase purity.

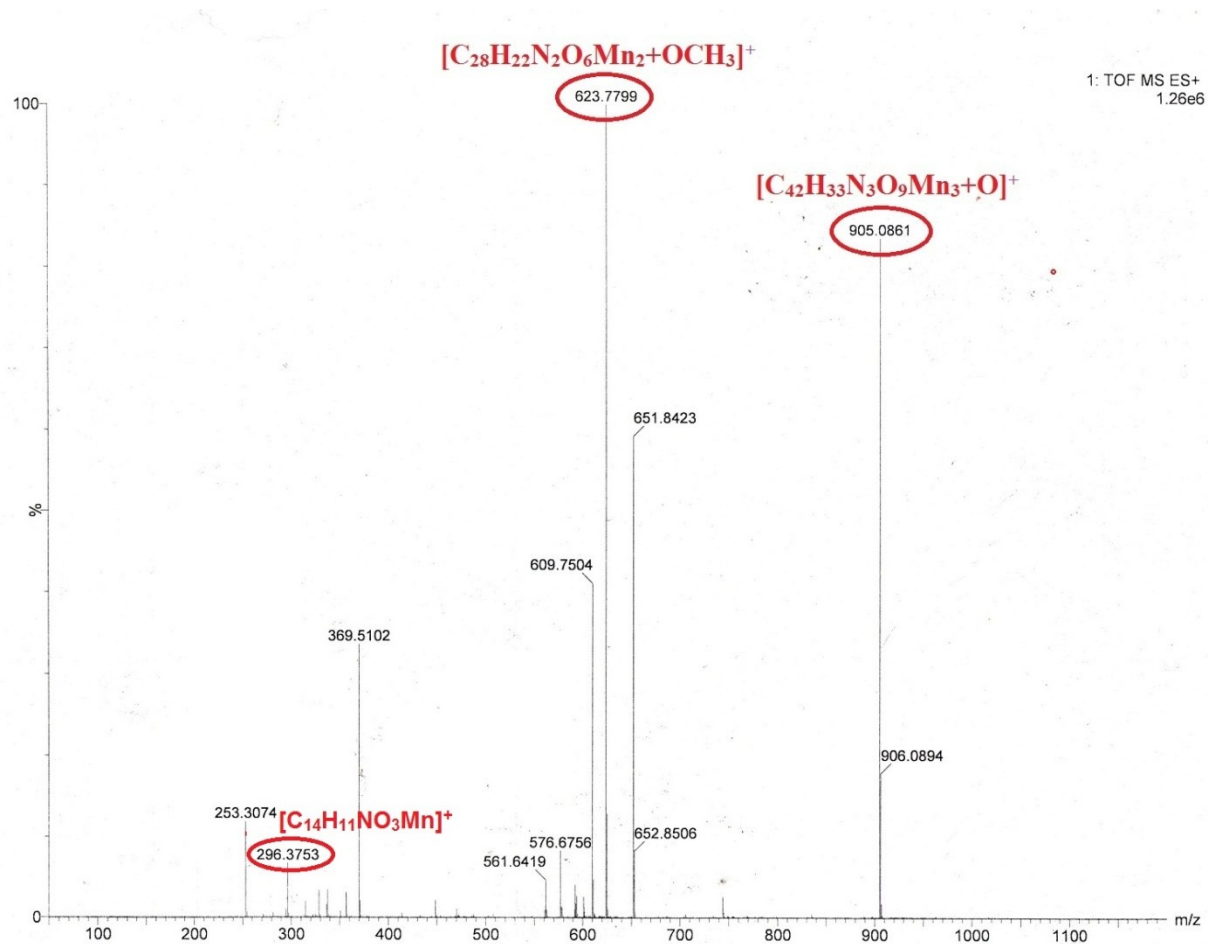


Figure S3. ESI-MS spectrum of complex **1** in methanol.

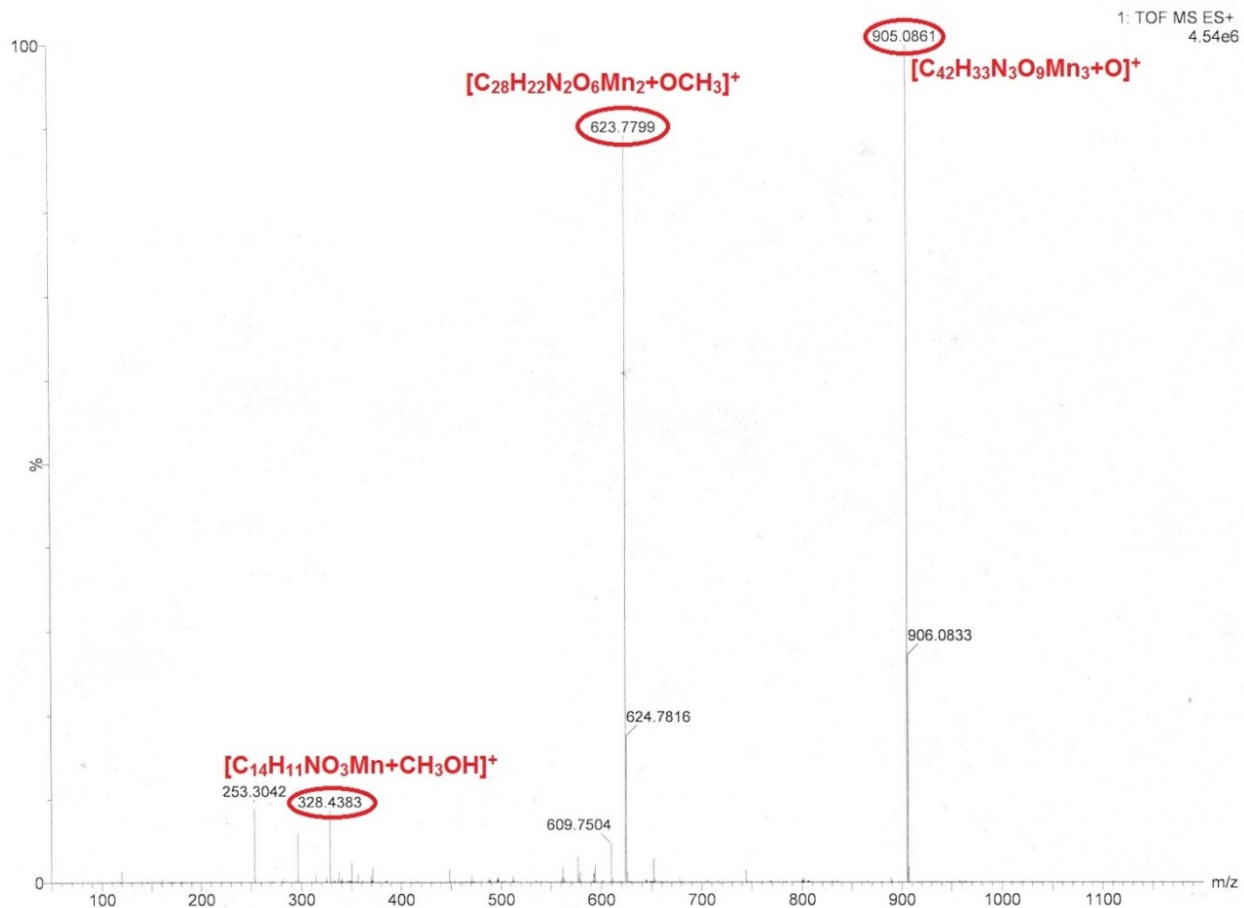


Figure S4. ESI-MS spectrum of complex **2** in methanol.

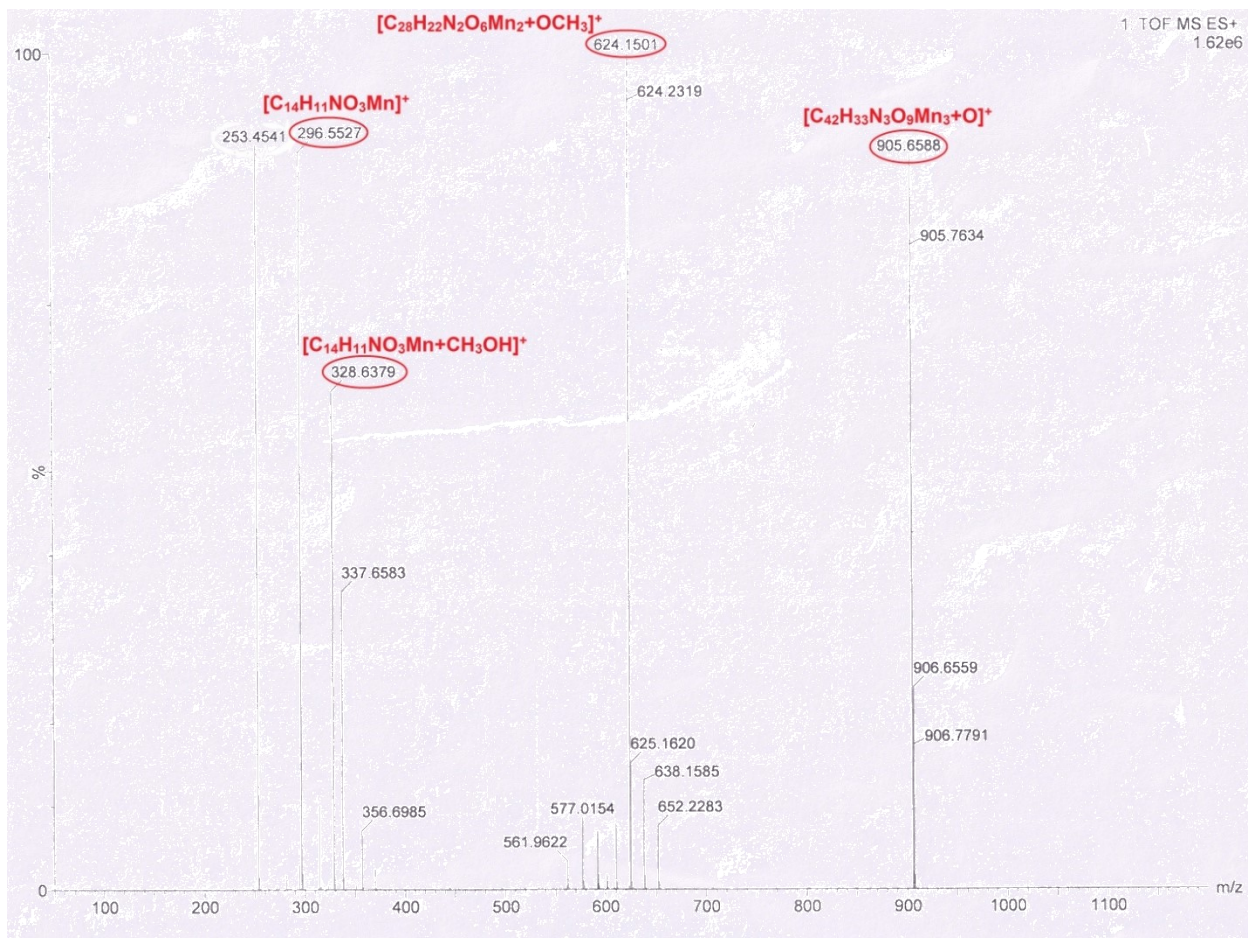


Figure S5. ESI-MS spectrum of complex **3** in methanol.

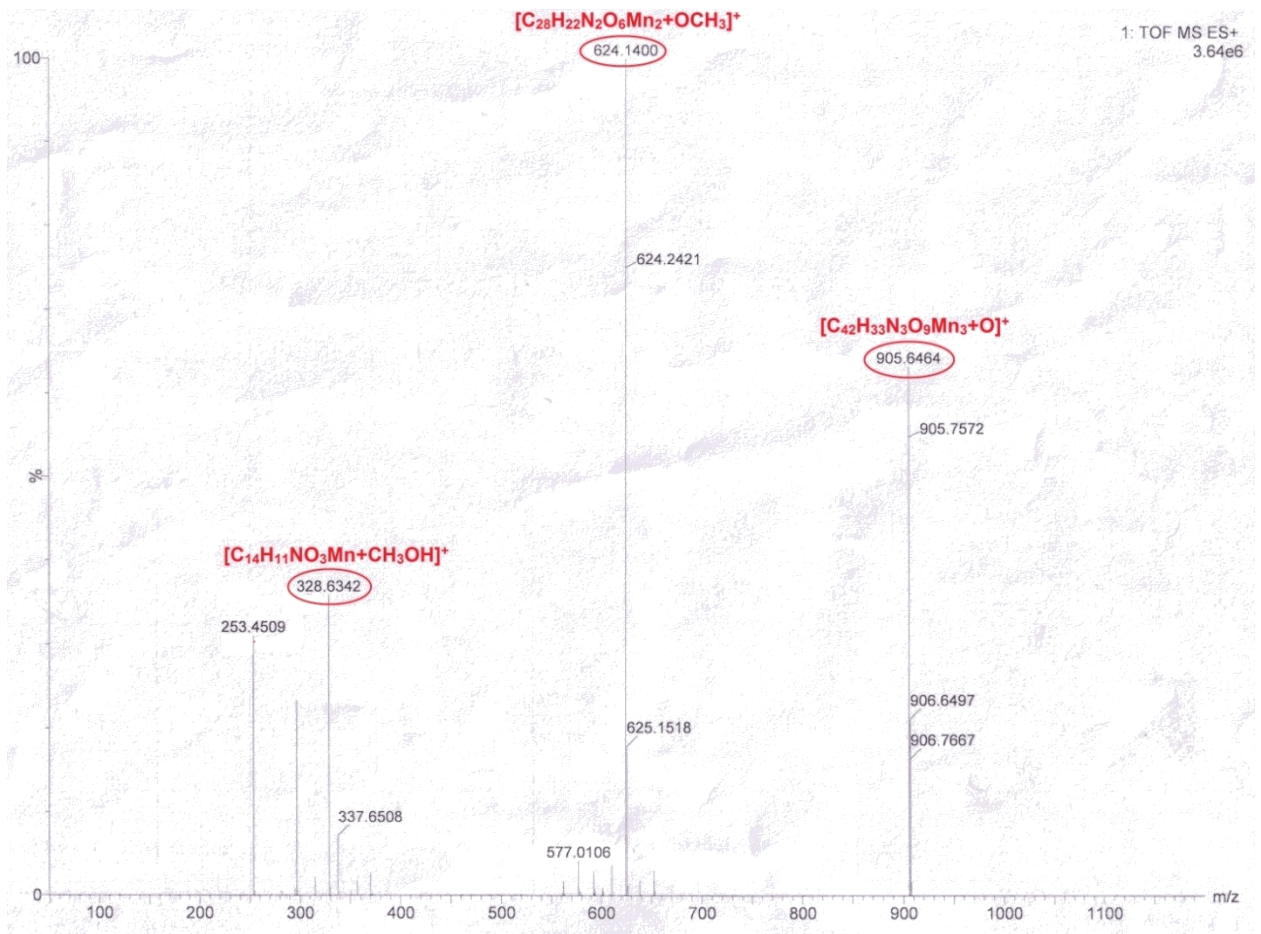


Figure S6. ESI–MS spectrum of complex **4** in methanol.

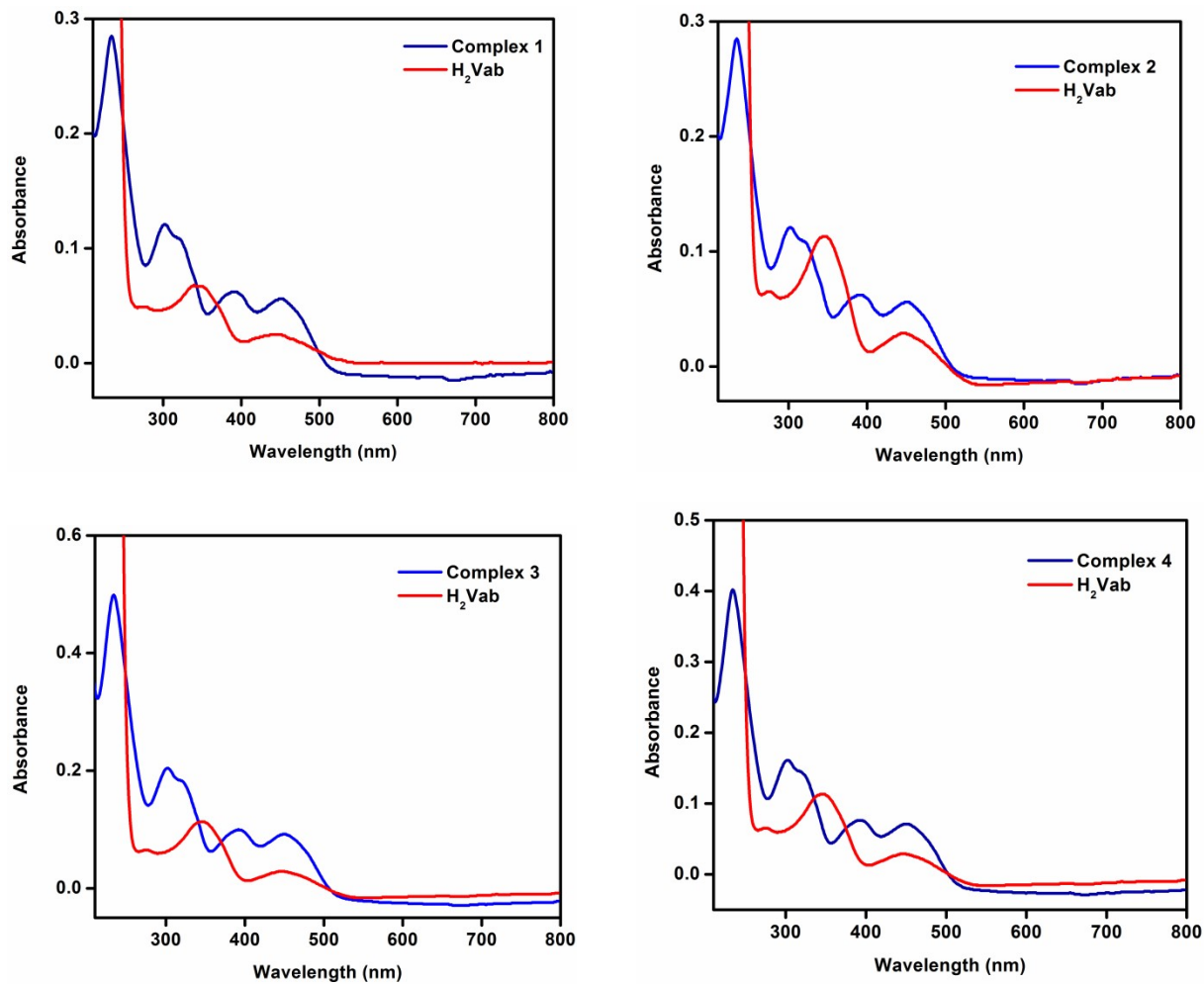


Figure S7. UV-Visible absorption spectra of complexes **1**, **2**, **3**, **4** and **H₂Vab**.

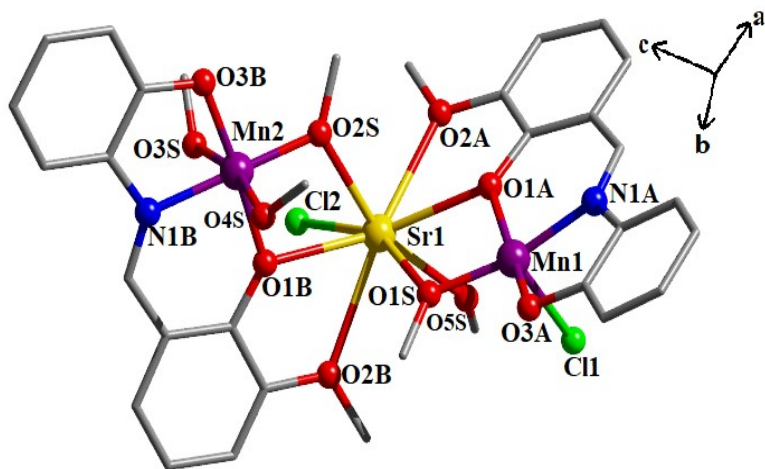


Figure S8. Crystal structure of complex **2** showing the trinuclear hetero-bimetallic core. Hydrogen atoms attached to carbon are removed for clarity. Color code: C = grey; N = blue; O = red; H = black; Cl = green; Mn^{III} = purple; Sr^{II} = gold.

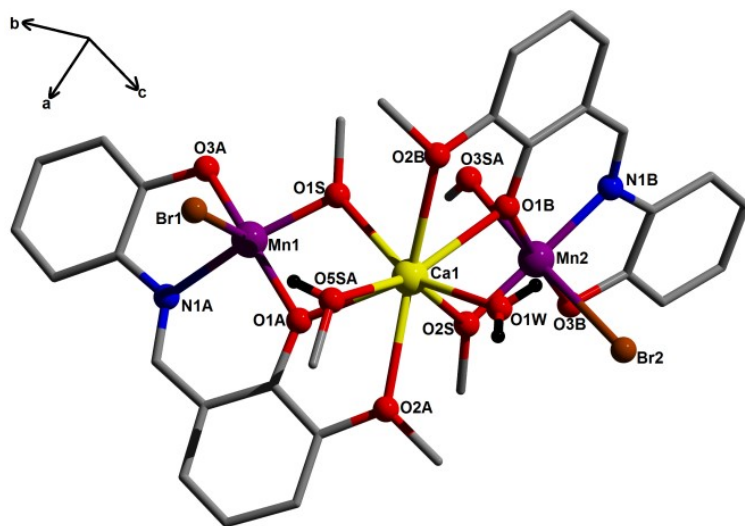


Figure S9. Crystal structure of complex **3** showing the trinuclear hetero-bimetallic core. Hydrogen atoms attached to carbon are removed for clarity. Color code: C = grey; N = blue; O = red; H = black; Br = brown; Mn^{III} = purple; Ca^{II} = yellow.

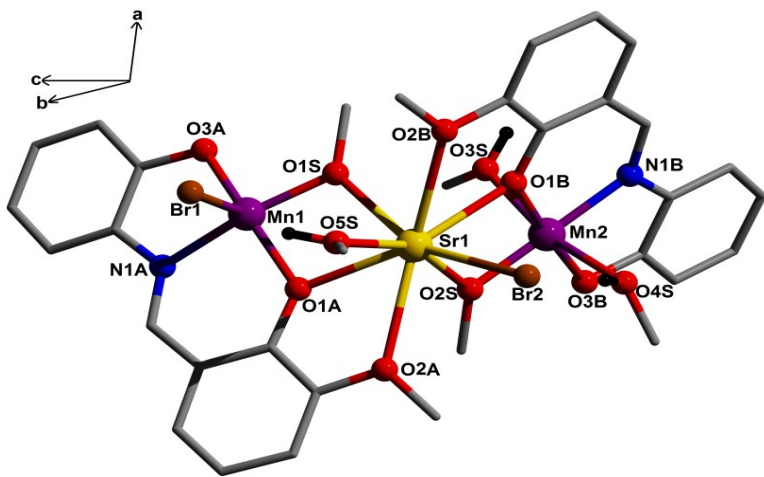


Figure S10. Crystal structure of complex **4** showing the trinuclear hetero-bimetallic core. Hydrogen atoms attached to carbon are removed for clarity. Color code: C = grey; N = blue; O = red; H = black; Br = brown; Mn^{III} = purple; Sr^{II} = gold.

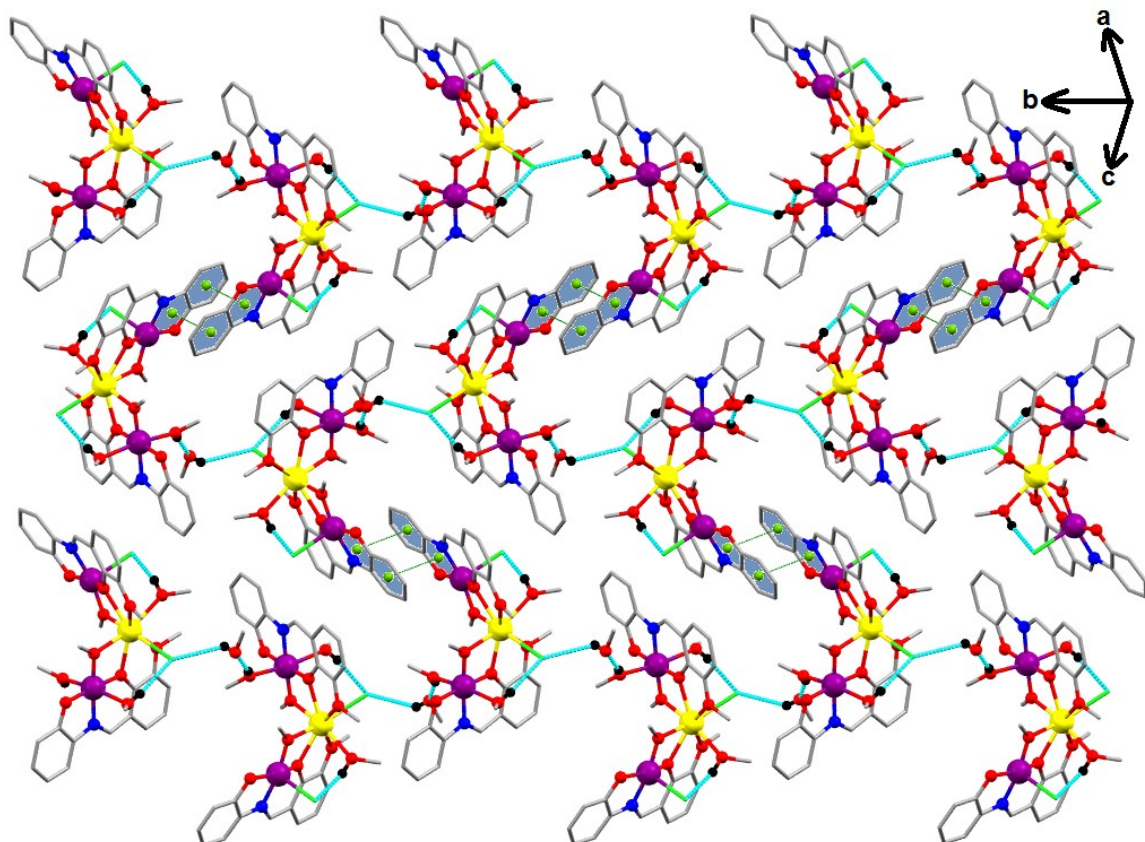


Figure S11. A supramolecular 2D structure of complex **1** formed by $\pi\cdots\pi$ interactions between 1D sheets along the *b* axis which are formed by O–H \cdots O bonds along the *a* axis.

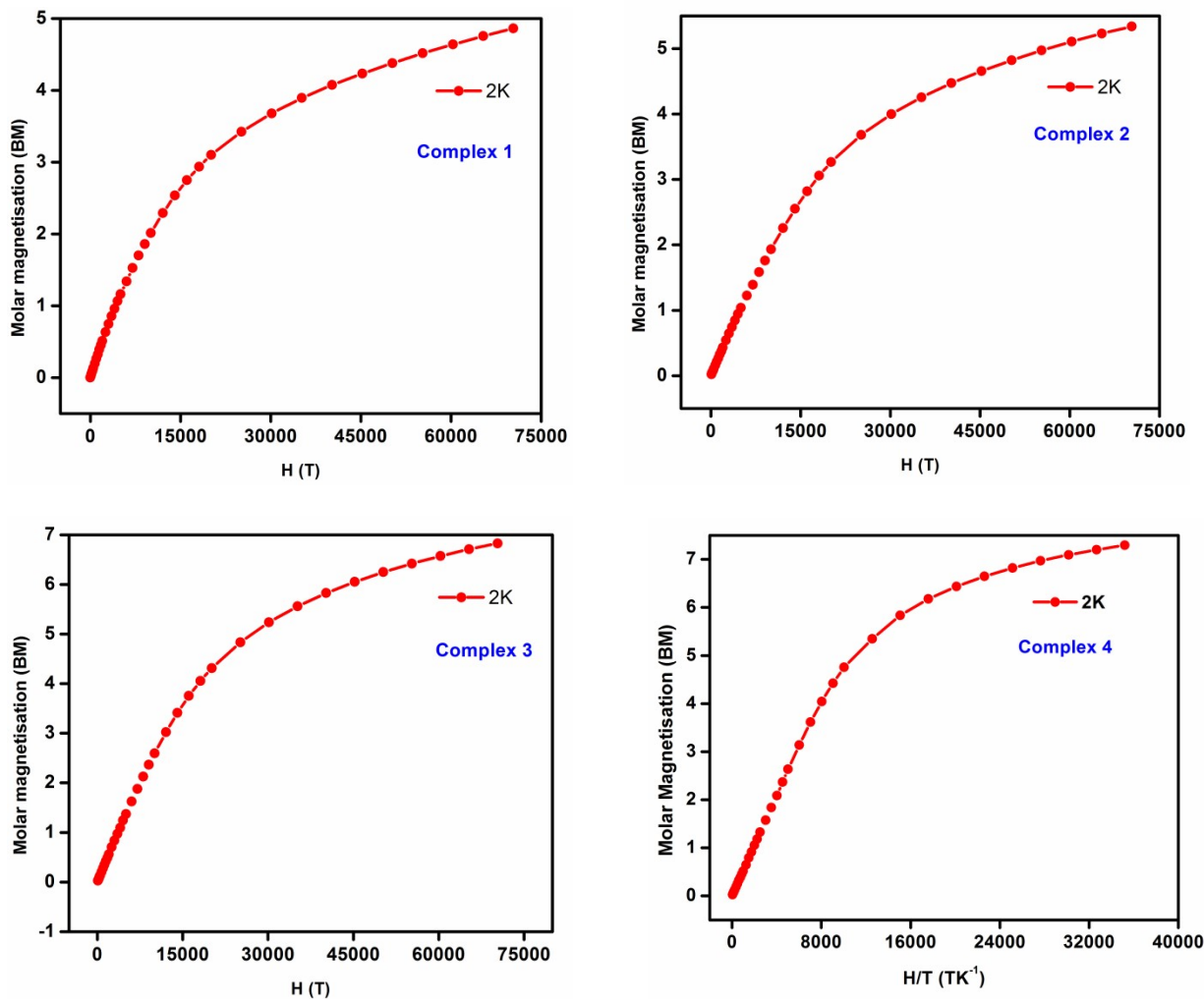


Figure S12. Molar magnetization (M) vs. magnetic field (H) for complexes **1-4** at 2.0 K.

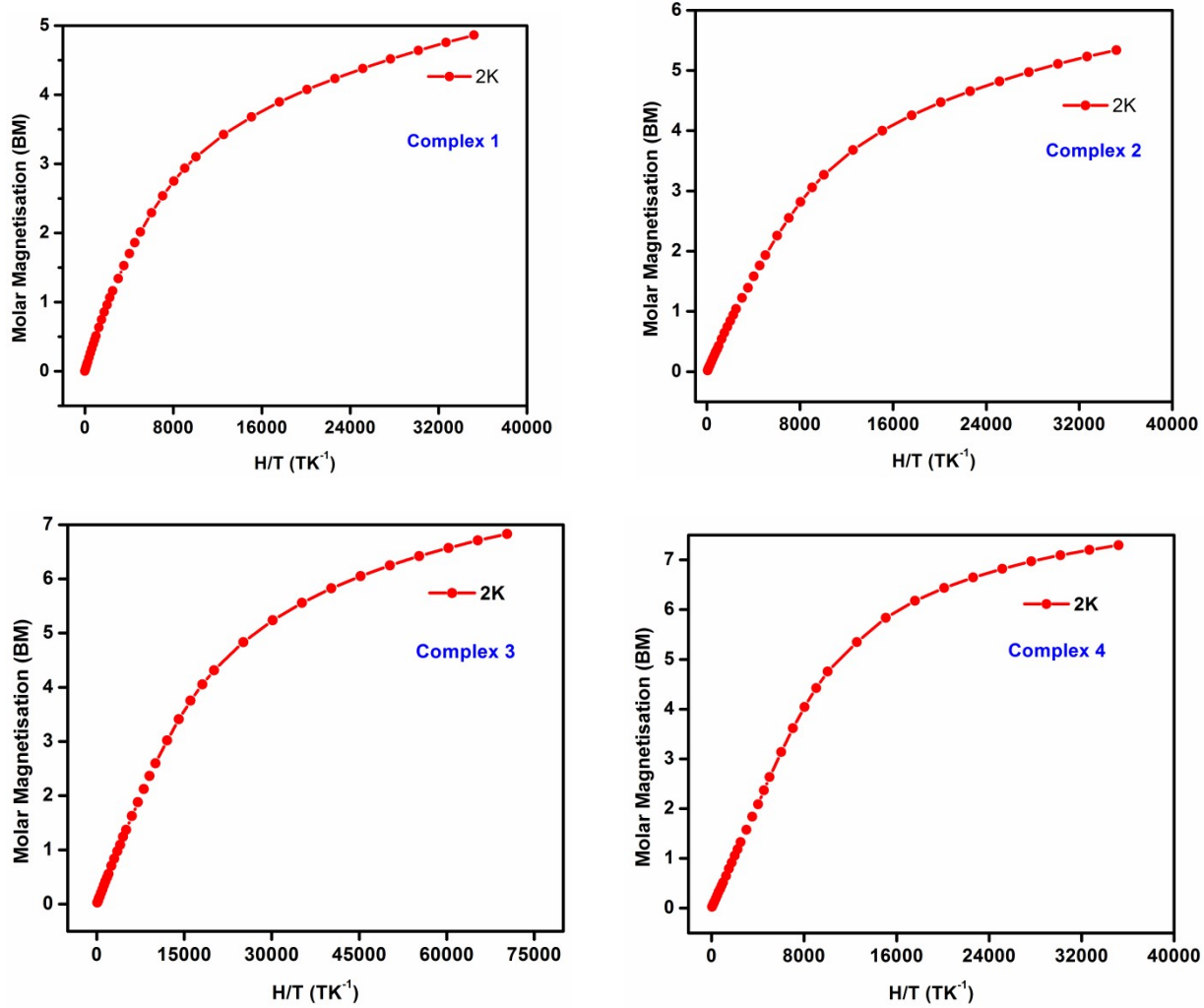


Figure S13. Molar magnetization (M) vs. H/T plot for complexes **1-4** at 2.0 K.

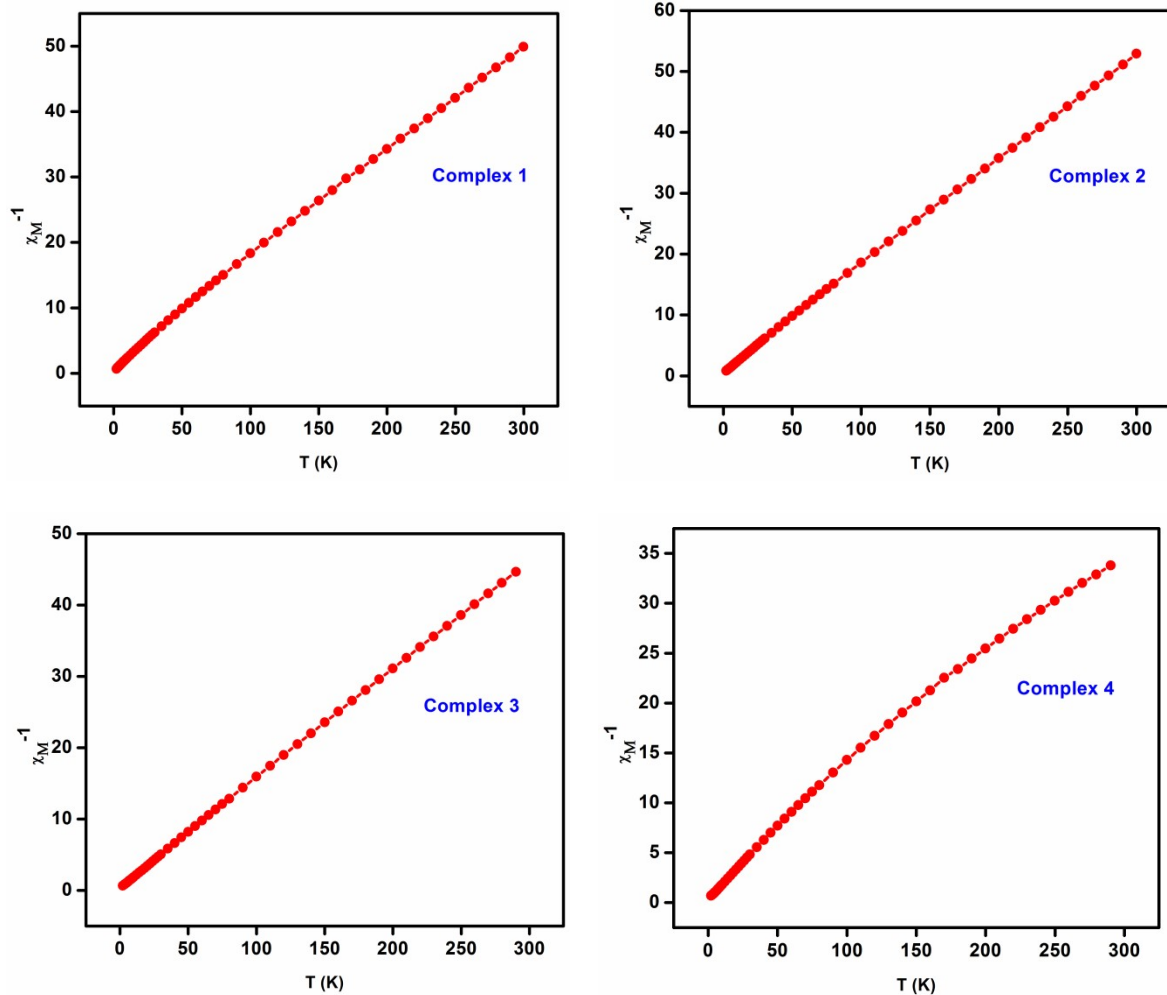


Figure S14. Temperature dependence of χ_M^{-1} for complexes **1-4**.

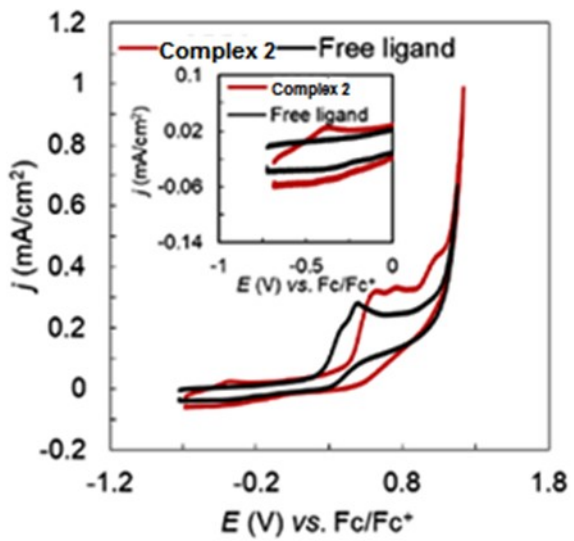


Figure S15. CV data for complex **2** (red) and its metal-free analog (black) in DMF. 3 mm glassy carbon as working, Ag/AgCl as a reference, Pt wire as a counter electrode.

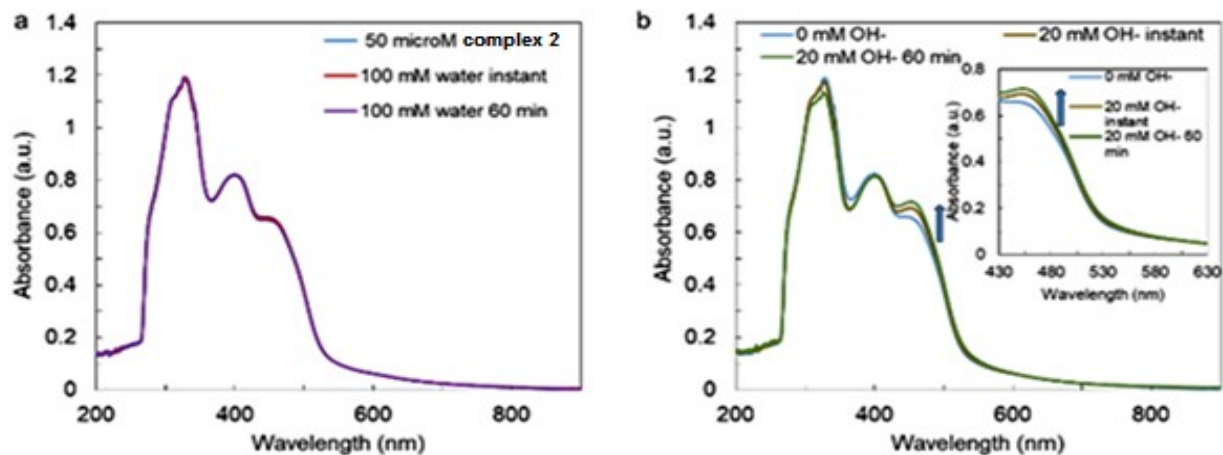


Figure S16. Comparative time-dependent UV-Visible spectra for complex **2**: a) after the addition of water and b) after the addition of OH^- .

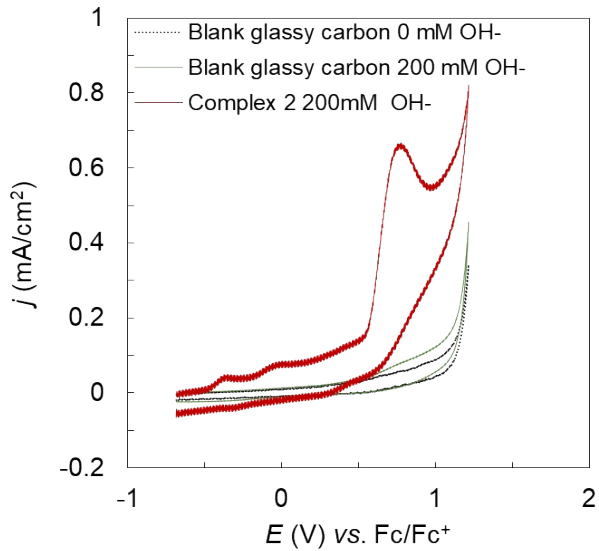


Figure S17. CV data for DMF with 200 mM OH⁻ with (red) and without the catalyst (complex **2**) (green) and only DMF (black dash). 3 mm glassy carbon as working, Ag/AgCl as a reference, Pt wire as a counter electrode.

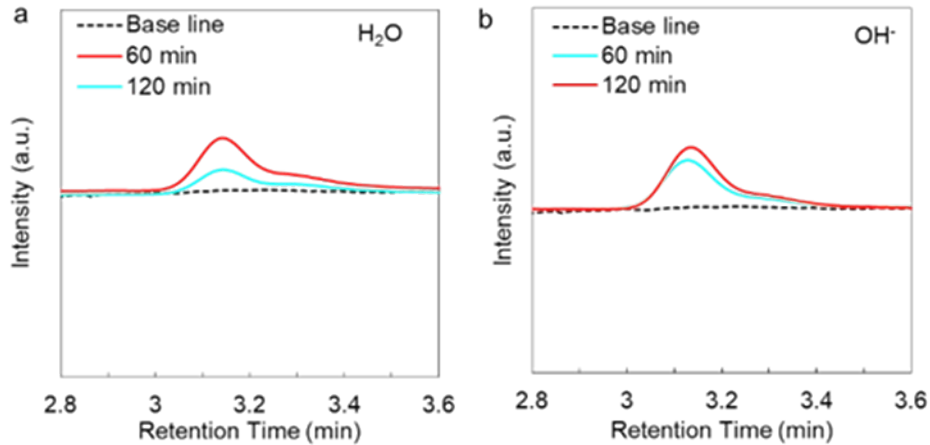


Figure S18. Gas chromatography (GC) Trace with complex **2**. a. Time-dependent GC trace for H₂O; b. OH⁻ oxidation. High surface area graphite rod as working, Ag/AgCl as a reference, Pt wire as a counter electrode. The controlled experiments without the manganese complex keeping all other experimental conditions unchanged (one with water and the other with hydroxide) yield no O₂ in GC. The current at the onset potential is very low. Hence, the electrolysis is performed

at a higher potential where the current density is large to ensure a detectable amount of O_2 production at a shorter time.

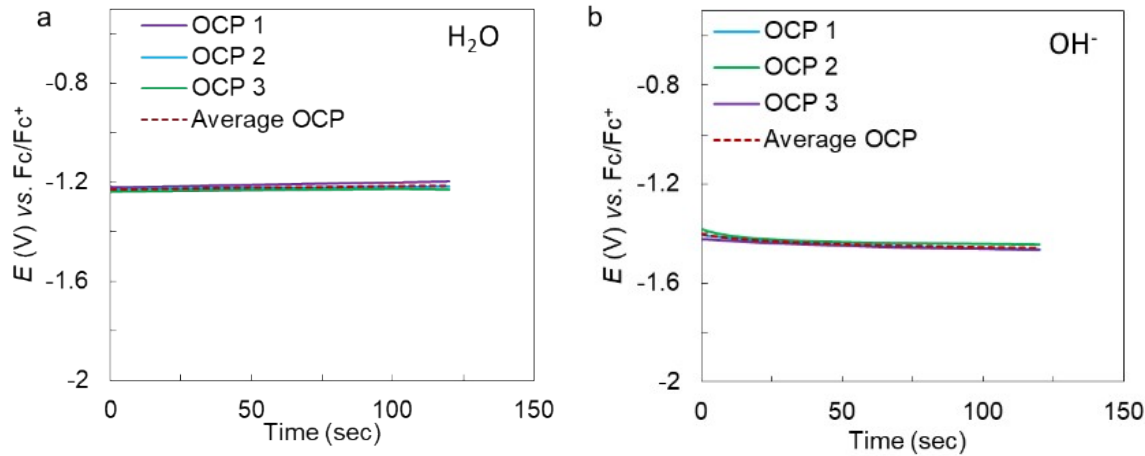


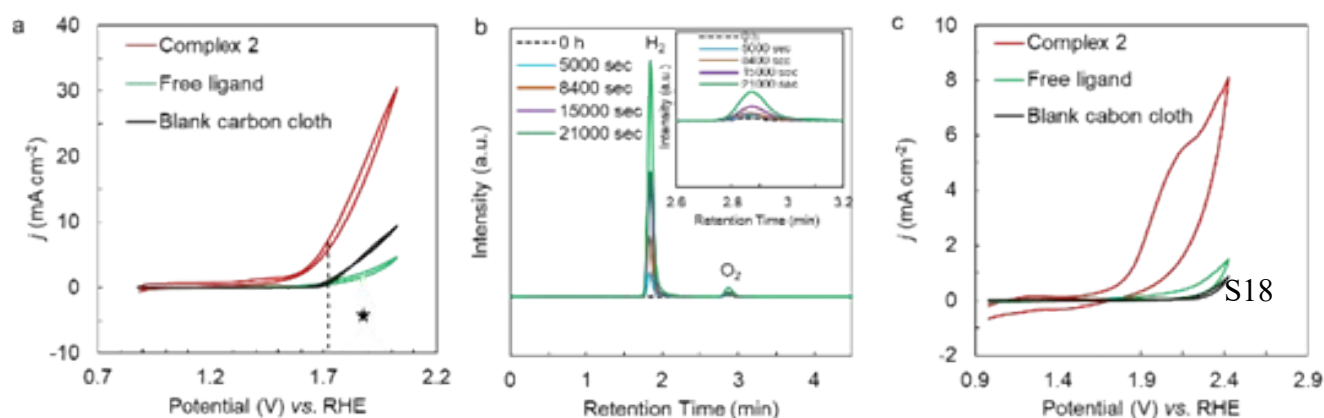
Figure S19. OCP measurement in DMF. a. OCP measurement with 1000 mM H_2O ; b. with 200 mM OH^- . Pt as working, Ag/AgCl as a reference, Pt wire as a counter electrode. The reference is corrected with respect to the $Fc^{+/0}$.

Figure S20. a. Comparative CV for complex 2, free ligand and blank carbon cloth in 1M KOH. b. Time-dependent GC trace for OH^- oxidation; c. Comparative CV for complex 2, free ligand, and blank carbon cloth in pH 7 buffer. The potential (1.75 V vs. RHE) at which electrolysis is performed is marked as an asterisk and the %FY is 77%.

1*1 cm² carbon cloth as working, Ag/AgCl as a reference, and Pt wire as a counter electrode. The catalyst ink is prepared in IPA with Nafion as a binder and in the presence of carbon black.

Table S1. Crystal refinement parameters of complexes 1-4.

	1	2	3	4
CCDC	2269162	2269163	2269164	2269165
Chemical formula	$C_{35}H_{48}CaCl_2$ $Mn_2N_2O_{13}$	$C_{33}H_{40}SrCl_2$ $Mn_2N_2O_{11}$	$C_{131.29}H_{171.18}Br_{8.70}$ $Ca_4Mn_8N_8O_{50.30}$	$C_{33}H_{40}SrBr_2$ $Mn_2N_2O_{11}$



Formula weight	925.61	909.07	3961.65	997.99
Crystal color, habit	brown, rectangular	brown, rectangular	brown, rectangular	brown, rectangular
Temperature (K)	296	296	100	100
λ^a Å	0.71073	0.71073	0.71073	0.71073
Crystal system	Monoclinic	Monoclinic	Monoclinic	Monoclinic
Space group	P2 ₁ /n	P2 ₁ /n	P2 ₁ /n	P2 ₁ /n
Unit cell dimensions				
a(Å)	14.317(1)	14.345(3)	14.2052(13)	14.2078(9)
b(Å)	18.4788(14)	18.298(4)	17.5541(15)	18.1152(13)
c(Å)	16.6261(12)	16.876(3)	16.6179(16)	16.8416(11)
α (deg)	90	90	90	90
β (deg)	104.813(3)	105.234(2)	103.820(3)	104.470(3)
γ (deg)	90	90	90	90
Volume(Å ³), Z	4252.4(5), 4	4274.0(15), 4	4023.9(6), 1	4197.1(5), 4
Density (mg m ⁻³)	1.446	1.413	1.635	1.579
Absolute coefficient (mm ⁻¹)	0.901	2.003	2.977	3.816
F(000)	1920.0	1848.0	2002.0	1992.0
θ range (deg)	1.678–25.396	1.662–25.143	2.056–26.372	2.023–30.508
Crystal size (mm)	0.36×0.30×0.24	0.24×0.18×0.13	0.23×0.18×0.07	0.24×0.22×0.20
Limiting indices	$-17 \leq h \leq 16$ $-22 \leq k \leq 21$ $-19 \leq l \leq 19$	$-16 \leq h \leq 16$ $-21 \leq k \leq 20$ $-19 \leq l \leq 20$	$-17 \leq h \leq 17$ $-21 \leq k \leq 21$ $-20 \leq l \leq 20$	$-20 \leq h \leq 20$ $-25 \leq k \leq 21$ $-24 \leq l \leq 24$
Reflections collected	55054	27418	86305	70748
Unique reflections (R _{int})	7753	7434	8205	12780
	0.0425	0.0496	0.0918	0.1086
Reflections with $I > 2\sigma(I)$	6568	5158	6061	8712
Completeness to θ	99.9 %	97.3 %	99.7 %	99.7 %
Completeness to θ	25.242	25.143	25.242	25.242
Data/Resistant/Paramet ers	7753 / 46 / 523	7434 / 33 / 487	8205 / 87 / 544	12780 / 9 / 476
GOOF on F2	1.068	1.149	1.101	1.022
Final R indices [I>2sigma(I)]	0.0474 ^b 0.1422 ^c	0.0404 ^b 0.1072 ^c	0.0872 ^b 0.2339 ^c	0.0407 ^b 0.0985 ^c
R indices (all data)	0.0567 ^b 0.1526 ^c	0.0853 ^b 0.1420 ^c	0.1166 ^b 0.2610 ^c	0.0835 ^b 0.1178 ^c
Max/Min residual peaks (e Å ⁻³)	0.950/-0.485	0.890/-1.224	2.178/-2.188	1.042/-1.515

^aGraphitemonochromator, ^bR₁ = $\sum(|F_o| - |F_c|)/\sum|F_o|$. ^cwR₂ = $\{\sum[w(|F_o|^2 - |F_c|^2)^2]/\sum[w(|F_o|^2)^2]\}^{1/2}$

Table S2. Selected bond lengths (Å) and bond angles (°) in complex **1**.

Bond lengths

Mn1–O1A	1.900(2)	Mn2–N1B	2.000(3)
Mn1–O3A	1.880(2)	Ca1–O1B	2.462(2)
Mn1–O1S	1.849(2)	Ca1–O2A	2.651(2)
Mn1–N1A	1.994(3)	Ca1–O1B	2.429(2)
Mn1–Cl1	2.4803(12)	Ca1–O2B	2.666(2)
Mn2–O1B	1.900(2)	Ca1–O1S	2.384(2)
Mn2–O3B	1.882(2)	Ca1–O2S	2.373(2)
Mn2–O2S	1.863(2)	Ca1–O5S	2.389(3)
Mn2–O3S	2.324(3)	Ca1–Cl2	2.8082(12)
Mn2–O4S	2.264(3)		

Bond angles			
O1S-Mn1-O3A	96.52(10)	O1S-Ca1-O5S	90.85(10)
O1S-Mn1-O1A	84.30(9)	O2S-Ca1-O1B	64.46(8)
O3A-Mn1-O1A	162.09(11)	O1S-Ca1-O1B	86.34(8)
O1S-Mn1-N1A	166.36(11)	O5S-Ca1-O1B	137.74(9)
O3A-Mn1-N1A	83.39(11)	O2S-Ca1-O1A	87.85(8)
O1A-Mn1-N1A	91.64(10)	O1S-Ca1-O1A	62.53(7)
O1S-Mn1-Cl1	100.68(9)	O5S-Ca1-O1A	76.19(9)
O3A-Mn1-Cl1	101.75(9)	O1B-Ca1-O1A	136.36(8)
O1A-Mn1-Cl1	95.65(8)	O2S-Ca1-O2A	79.63(8)
N1A-Mn1-Cl1	92.66(8)	O1S-Ca1-O2A	123.08(8)
O2S-Mn2-O3B	97.86(10)	O5S-Ca1-O2A	78.57(10)
O2S-Mn2-O1B	85.78(10)	O1B-Ca1-O2A	136.26(8)
O3B-Mn2-O1B	176.36(10)	O1A-Ca1-O2A	60.61(7)
O2S-Mn2-N1B	177.26(11)	O2S-Ca1-O2B	124.96(8)
O3B-Mn2-N1B	84.33(11)	O1S-Ca1-O2B	76.13(8)
O1B-Mn2-N1B	92.03(10)	O5S-Ca1-O2B	77.63(9)
O2S-Mn2-O4S	97.26(14)	O1B-Ca1-O2B	60.75(7)
O1B-Mn2-O4S	89.00(12)	O1A-Ca1-O2B	129.98(8)

N1B-Mn2-O4S	84.34(13)	O2A-Ca1-O2B	149.49(8)
O2S-Mn2-O3S	93.00(12)	O2S-Ca1-Cl2	96.21(7)
O3B-Mn2-O3S	93.05(11)	O1S-Ca1-Cl2	154.29(7)
O1B-Mn2-O3S	86.50(11)	O5S-Ca1-Cl2	86.52(8)
N1B-Mn2-O3S	85.22(11)	O1B-Ca1-Cl2	78.65(6)
O4S-Mn2-O3S	168.47(13)	O1A-Ca1-Cl2	140.51(6)
O2S-Ca1-O1S	95.96(10)	O2A-Ca1-Cl2	81.44(6)
O2S-Ca1-O5S	157.36(10)	O2B-Ca1-Cl2	78.33(7)

Table S3. Selected bond lengths (\AA) and bond angles ($^\circ$) in complex **2**.

Bond lengths			
Mn1–O1A	1.898(3)	Mn2–N1B	1.989(4)
Mn1–O3A	1.874(3)	Sr1–O1A	2.587(3)
Mn1–O1S	1.842(3)	Sr1–O2A	2.700(3)
Mn1–N1A	1.991(4)	Sr1–O1B	2.562(3)
Mn1–Cl1	2.4714(14)	Sr1–O2B	2.726(3)
Mn2–O1B	1.908(3)	Sr1–O1S	2.505(3)
Mn2–O3B	1.875(3)	Sr1–O2S	2.513(3)
Mn2–O2S	1.856(3)	Sr1–O5S	2.543(3)
Mn2–O3S	2.313(3)	Sr1–Cl2	2.9216(14)
Mn2–O4S	2.243(4)		

Bond angles			
O1S-Mn1-O3A	96.03(14)	O2S-Sr1-O5S	160.47(13)
O1S-Mn1-O1A	85.37(13)	O1S-Sr1-O1B	88.62(10)
O3A-Mn1-O1A	162.66(14)	O2S-Sr1-O1B	61.78(10)
O1S-Mn1-N1A	165.98(14)	O5S-Sr1-O1B	137.66(12)
O3A-Mn1-N1A	83.25(15)	O1S-Sr1-O1A	59.70(10)
O1A-Mn1-N1A	91.22(14)	O2S-Sr1-O1A	89.75(9)
O1S-Mn1-Cl1	100.27(11)	O5S-Sr1-O1A	75.31(10)
O3A-Mn1-Cl1	101.27(11)	O1B-Sr1-O1A	136.18(9)
O1A-Mn1-Cl1	95.45(9)	O1S-Sr1-O2A	118.31(9)
N1A-Mn1-Cl1	93.59(10)	O2S-Sr1-O2A	81.40(10)
O2S-Mn2-O3B	96.41(14)	O5S-Sr1-O2A	80.09(13)
O2S-Mn2-O1B	87.62(13)	O1B-Sr1-O2A	136.71(9)
O3B-Mn2-O1B	175.76(14)	O1A-Sr1-O2A	58.72(9)
O2S-Mn2-N1B	178.30(15)	O1S-Sr1-O2B	77.01(10)
O3B-Mn2-N1B	84.17(15)	O2S-Sr1-O2B	119.91(10)
O3B-Mn2-N1B	91.76(14)	O5S-Sr1-O2B	79.60(12)
O2S-Mn2-O4S	96.47(15)	O1B-Sr1-O2B	58.59(9)

O3B-Mn2-O4S	91.49(16)	O1A-Sr1-O2B	129.88(10)
O1B-Mn2-O4S	89.38(15)	O2A-Sr1-O2B	154.03(10)
N1B-Mn2-O4S	85.10(15)	O1S-Sr1-Cl2	157.21(8)
O2S-Mn2-O3S	92.59(15)	O2S-Sr1-Cl2	95.48(8)
O3B-Mn2-O3S	92.75(14)	O5S-Sr1-Cl2	88.52(8)
O1B-Mn2-O3S	85.71(13)	O1B-Sr1-Cl2	78.77(7)
N1B-Mn2-O3S	85.78(15)	O1A-Sr1-Cl2	140.39(8)
O4S-Mn2-O3S	169.51(15)	O2A-Sr1-Cl2	83.25(7)
O1S-Sr1-O2S	95.12(11)	O2B-Sr1-Cl2	80.21(8)
O1S-Sr1-O5S	88.20(12)		

Table S4. Selected bond lengths (\AA) and bond angles ($^\circ$) in complex **3**.

Bond lengths			
Mn1–O1	1.874(5)	Mn2–N3	2.261(9)
Mn1–O2	1.886(5)	Ca1–O1W	2.366(7)
Mn1–O5	1.874(5)	Ca1–O2	2.412(5)
Mn1–N1	2.001(6)	Ca1–O2W	2.401(6)
Mn1–Br	2.6604(14)	Ca1–O4	2.422(5)
Mn2–O3	1.878(5)	Ca1–O5	2.438(5)
Mn2–O3W	2.308(7)	Ca1–O6	2.370(5)
Mn2–O4	1.900(5)	Ca1–O7	2.550(6)
Mn2–O6	1.859(6)	Ca1–O8	2.602(7)
Mn2–O7	2.261(9)		

Bond angles			
O1-Mn1-O2	164.8(2)	O1W-Ca1-O4	80.1(2)
O1-Mn1-O5	96.2(2)	O1W-Ca1-O5	155.0(2)
O1-Mn1-N1	84.0(2)	O1W-Ca1-O6	96.0(2)
O2-Mn1-O5	84.2(2)	O1W-Ca1-N2	80.1(2)
O2-Mn1-N1	92.0(2)	O1W-Ca1-N4	78.5(3)
O5-Mn1-N1	166.2(2)	O2-Ca1-O2W	77.2(2)
O1-Mn1-Br1	99.57(16)	O2-Ca1-O4	135.96(18)
O2-Mn1-Br1	95.27(16)	O2-Ca1-O5	62.60(16)
O5-Mn1-Br1	100.71(16)	O2-Ca1-O6	89.08(18)
N1-Mn1-Br1	92.85(15)	O2-Ca1-N2	62.60(16)
O3-Mn2-O3W	95.0(2)	O2-Ca1-N4	128.58(19)
O3-Mn2-O4	175.5(2)	O2W-Ca1-O4	138.9(2)
O3-Mn2-O6	98.7(2)	O2W-Ca1-O5	98.6(2)
O3-Mn2-O7	92.2(3)	O2W-Ca1-O6	154.3(2)
O3-Mn2-N3	84.2(2)	O2W-Ca1-N2	77.1(2)
O3W-Mn2-O4	84.9(2)	O2W-Ca1-N4	78.9(2)
O3W-Mn2-O4	86.7(3)	O4-Ca1-O5	83.67(17)

O3W-Mn2-O7	172.3(3)	O4-Ca1-O6	64.56(19)
O3W-Mn2-N3	94.0(3)	O4-Ca1-N2	134.45(17)
O4-Mn2-O6	85.8(2)	O4-Ca1-N4	61.51(19)
O4-Mn2-O7	87.8(3)	O5-Ca1-O6	94.00(18)
O4-Mn2-N3	91.3(2)	O5-Ca1-N2	124.56(17)
O6-Mn2-O7	95.0(3)	O5-Ca1-N4	77.05(19)
O6-Mn2-N3	177.0(2)	O6-Ca1-N2	77.32(19)
O7-Mn2-N3	83.9(3)	O6-Ca1-N4	125.9(2)
O1W-Ca1-O2	140.3(2)	N2-Ca1-N4	149.8(2)
O1W-Ca1-O2W	81.8(2)		

Table S5. Selected bond lengths (Å) and bond angles (°) in complex **4**.

Bond lengths			
Mn1-O4	1.850(2)	Mn2-N2	2.006(3)
Mn1-O1	1.876(2)	Sr1-O9	2.501(2)
Mn1-O2	1.904(2)	Sr1-O4	2.505(2)
Mn1-N1	1.998(3)	Sr1-O7	2.543(2)
Mn1-N1	2.6749(6)	Sr1-O5	2.554(2)
Mn2-O9	1.875(2)	Sr1-O2	2.571(2)
Mn2-O6	1.885(2)	Sr1-O3	2.688(2)
Mn2-O7	1.909(2)	Sr1-O8	2.692(2)
Mn2-O10	2.231(3)	Sr1-Br2	3.1324(5)
Mn2-O11	2.307(3)		

Bond angles			
O4-Mn1-O1	96.21(10)	O4-Sr1-O7	88.03(7)
O4-Mn1-O2	85.65(10)	O9-Sr1-O5	159.44(8)
O1-Mn1-O2	166.97(10)	O4-Sr1-O5	94.82(8)
O4-Mn1-N1	166.41(11)	O7-Sr1-O5	135.81(8)
O1-Mn1-N1	83.73(10)	O9-Sr1-O2	92.29(8)
O2-Mn1-N1	91.45(10)	O4-Sr1-O2	60.35(7)
O4-Mn1-Br1	98.58(8)	O7-Sr1-O2	138.06(7)
O1-Mn1-Br1	98.71(7)	O5-Sr1-O2	77.80(8)
O2-Mn1-Br1	93.74(7)	O9-Sr1-O3	80.45(8)
N1-Mn1-Br1	94.85(8)	O4-Sr1-O3	119.11(7)
O9-Mn2-O6	97.04(10)	O7-Sr1-O3	136.39(7)
O9-Mn2-O7	87.07(10)	O5-Sr1-O3	79.00(8)
O6-Mn2-O7	175.87(10)	O2-Sr1-O3	59.15(7)
O9-Mn2-N2	177.29(12)	O9-Sr1-O8	120.91(7)
O6-Mn2-N2	84.31(11)	O4-Sr1-O8	74.78(7)
O7-Mn2-N2	91.56(10)	O7-Sr1-O8	59.31(7)

O9-Mn2-O10	95.36(11)	O5-Sr1-O8	78.93(8)
O6-Mn2-O10	92.80(10)	O2-Sr1-O8	126.69(7)
O7-Mn2-O10	87.18(10)	O3-Sr1-O8	154.82(7)
N2-Mn2-O10	86.91(11)	O9-Sr1-Br2	93.19(6)
O9-Mn2-O11	92.29(10)	O4-Sr1-Br2	156.22(5)
O6-Mn2-O11	93.30(10)	O7-Sr1-Br2	76.79(5)
O7-Mn2-O11	86.12(9)	O5-Sr1-Br2	83.97(6)
N2-Mn2-O11	85.28(10)	O2-Sr1-Br2	141.25(5)
O10-Mn2-O11	169.56(10)	O3-Sr1-Br2	84.07(5)
O9-Sr1-O4	95.79(8)	O8-Sr1-Br2	81.70(5)
O9-Sr1-O7	62.22(7)		

Table S6. Bond Valence Sum (BVS) results for manganese centers in complex **1** in different oxidation states and their assignment.

	Mn^{II}	Mn^{III}	Assignment
Mn1	3.271	3.084	Mn^{III}
Mn2	3.314	3.082	Mn^{III}

Table S7. Bond Valence Sum (BVS) results for manganese centers in complex **2** in different oxidation states and their assignment.

	Mn^{II}	Mn^{III}	Assignment
Mn1	3.387	3.149	Mn^{III}
Mn2	3.315	3.125	Mn^{III}

Table S8. Bond Valence Sum (BVS) results for manganese centers in complex **3** in different oxidation states and their assignment.

	Mn^{II}	Mn^{III}	Assignment
Mn1	3.114	2.969	Mn^{III}
Mn2	3.504	3.321	Mn^{III}

Table S9. Bond Valence Sum (BVS) results for manganese centers in complex **4** in different oxidation states and their assignment.

	Mn^{II}	Mn^{III}	Assignment
Mn1	3.139	2.997	Mn^{III}
Mn2	3.464	3.288	Mn^{III}

Table S10. Continuous Shape Measures (CShMs) of manganese centers in complexes **1**, **2**, **3** and **4** respectively relative to ideal 5/6-vertex polyhedral. The lowest CShMs value which corresponds to closest geometry is highlighted.

5–vertex polyhedral						
Mn1						
	Complex1	Complex2	Complex3	Complex4	Symmetry	Ideal shape
PP-5	31.349	29.510	32.128	32.981	D5h	Pentagon
vOC-5	2.669	2.291	3.408	3.298	D5h	Vacant octahedron
TBPY-5	5.298	6.516	6.040	6.231	D3h	Trigonalbipyramidal
SPY-5	0.870	1.529	1.264	1.238	C4v	Spherical square pyramid
JTBPY-5	8.808	7.473	9.737	10.210	D3h	Johnson trigonalbipyramidal J12

6–vertex polyhedral						
Mn2						
	Complex1	Complex2	Complex3	Complex4	Symmetry	Ideal shape
HP-6	31.933	28.041	30.680	31.993	D6h	Hexagon
PPY-6	27.384	27.172	27.826	27.936	C5v	Pentagonal pyramid
OC-6	1.091	2.884	1.091	0.888	Oh	Octahedron
TPR-6	14.890	14.982	15.986	15.018	D3h	Trigonal prism
JPPY-6	30.347	29.841	30.522	30.981	C5v	Johnson pentagonal pyramid J2

Table S11. Continuous Shape Measures (CShMs) of calcium and strontium centers in complexes **1**, **3** and **2**, **4** respectively relative to ideal 8–vertex polyhedral. The lowest CShMs value which corresponds to closest geometry is highlighted.

8–vertex polyhedral						
Ca1						

	Complex1	Complex3	Symmetry	Ideal shape
OP-8	31.782	31.367	D8h	Octagon
HPY-8	24.413	23.402	C7v	Heptagonal pyramid
HPY-8	13.019	12.854	D6h	Hexagonal bipyramid
CU-8	10.810	10.103	Oh	Cube
SAPR-8	4.566	3.622	D4d	Square antiprism
TDD-8	3.030	2.742	D2d	Triangular dodecahedron
JGBF-8	11.268	10.788	D2d	Johnson gyrobifastigium J26
JETBPY-8	26.374	25.043	D3h	Johnson elongated triangular bipyramid J14
JBTPR-8	3.868	3.363	C2v	Biaugmentedtrigonal prism J50
BTPR-8	3.428	2.970	C2v	Biaugmentedtrigonal prism
JSD-8	3.745	3.322	D2d	Snub diphenoïd J84
TT-8	11.180	10.933	TT-8	Triakis tetrahedron
ETBPY-8	22.864	22.451	D3h	Elongated trigonalbipyramid

8–vertex polyhedral

	Sr1			
	Complex2	Complex4	Symmetry	Ideal shape
OP-8	26.281	32.759	D8h	Octagon
HPY-8	21.210	23.126	C7v	Heptagonal pyramid
HPY-8	12.474	12.149	D6h	Hexagonal bipyramid

CU-8	11.733	9.709	Oh	Cube
SAPR-8	7.905	5.214	D4d	Square antiprism
TDD-8	5.636	4.264	D2d	Triangular dodecahedron
JGBF-8	11.562	12.139	D2d	Johnson gyrobiastigium J26
JETBPY-8	17.623	25.848	D3h	Johnson elongated triangular bipyramid J14
JBTPR-8	4.568	5.294	C2v	Biaugmentedtrigonal prism J50
BTPR-8	5.875	4.642	C2v	Biaugmentedtrigonal prism
JSD-8	4.892	5.452	D2d	Snub diphenoid J84
TT-8	12.279	10.009	TT-8	Triakis tetrahedron
ETBPY-8	19.162	20.540	D3h	Elongated trigonalbipyramide

Table S12. Hydrogen bond parameters found in complex **1**, (distances (Å), angles, (°)).

Donor–H···Acceptor	D–H	H···A	D···A	D–H···A
O5S–H5S···Cl1	0.93	2.18	3.089(3)	165
O6S–H6S···Cl2	0.82	2.59	3.308(9)	147
O7S–H7S···Cl2	0.82	2.74	3.169(7)	114

O3S–H3S···Cl2	0.809(19)	2.36(2)	3.160(3)	171(5)
O4S–H4S···O7S	0.83(2)	1.93(3)	2.725(8)	159(6)

Table S13. Hydrogen bond parameters found in complex **2**, (distances (Å), angles, (°)).

Donor–H···Acceptor	D–H	H···A	D···A	D–H···A
O5S–H5SO···Cl1	0.88(2)	2.22(2)	3.088(4)	172(4)
O3S–H3SO···Cl2	0.886(14)	2.50(4)	3.203(4)	137(4)

Table S14. Hydrogen bond parameters found in complex **3**, (distances (Å), angles, (°)).

Donor–H···Acceptor	D–H	H···A	D···A	D–H···A
O2W–H2W···Br1	0.82(4)	2.46(3)	3.236(6)	159(6)
O3W–H3W2···O5	0.80(3)	2.39(6)	3.061(9)	141(9)

Table S15. Hydrogen bond parameters found in complex **4**, (distances (Å), angles, (°)).

Donor–H···Acceptor	D–H	H···A	D···A	D–H···A
O11–H11C···Br2	0.75	2.54	3.249(3)	157.0

Table S16. Electrochemical parameters for manganese complexes used in this study.

Complexes	Redox I	Redox II	i_c / i_p	i_c / i_p
	($E_{1/2}$ V vs. Fc/Fc ⁺)	(E_a V vs. Fc/Fc ⁺)	(1 M H ₂ O)	(0.2 M OH ⁻)
1	-0.43	0.58	18.90	24.00
2	-0.40	0.61	21.42	29.46

3	-0.39	0.40	—	22.17
4	-0.40	0.38	—	20.80

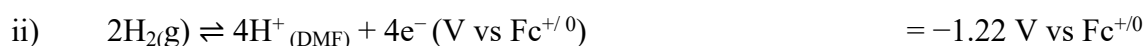
Table S17. Over potential values of different complexes based on the OCP values.

SL no.	complexes	Over potential, water	Over potential, hydroxide
		oxidation	oxidation
1	Complex 1	569 mV	822 mV
2	Complex 2	557 mV	851 mV
3	Complex 3	-	754 mV
4	Complex 4	-	741 mV

The detailed calculation is provided below:

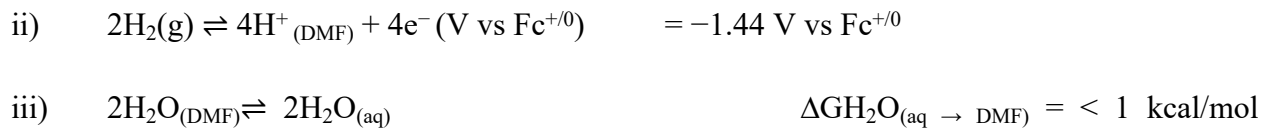
Estimation of E_{O_2/H_2O} based on EH^+/H_2 measured by OCP:

The reduction potential for O_2/H_2O in DMF containing 1000mM water may be estimated using i) the standard aqueous cell potential for $O_2 + H_2 \rightarrow H_2O$, ii) the measurement of the open circuit potential (OCP) for H^+/H_2 (EH^+/H_2), and iii) the Gibbs free energy to transfer H_2O from H_2O to DMF. It may be calculated by the following equations:



The reduction potential for O_2/H_2O in DMF containing 200 mM KOH may be estimated using i) the standard aqueous cell potential for $O_2 + H_2 \rightarrow H_2O$, ii) the measurement of the open circuit potential (OCP) for H^+/H_2 (EH^+/H_2), and iii) the Gibbs free energy to transfer H_2O from H_2O to DMF. It may be calculated by the following equations:





$$\text{Overpotential} = |\text{E}_{\text{cat}/2} - \text{EO}_2/\text{H}_2\text{O}_{(\text{DMF})}|$$

Table S18. OER half-wave potential of complexes with respect to NHE calculated using equation 3.¹

SL no.	complexes	<i>E</i> _{cat/2} vs. NHE, water	<i>E</i> _{cat/2} vs. NHE, hydroxide
		oxidation	oxidation
1	Complex 1	1.290 V	1.323 V
2	Complex 2	1.278 V	1.352 V
3	Complex 3	-	1.255 V
4	Complex 4	-	1.242 V

$$E_{\text{NHE}} = E_{\text{SCE}} + 0.241 \text{ V} \quad \text{equation 1}$$

$$E_{\text{Fc/Fc}^+} = 0.47 \text{ V vs. SCE} \quad \text{equation 2}$$

$$E_{\text{NHE}} = E_{\text{Fc/Fc}^+} + 0.241 \text{ V} + 0.47 \text{ V} \quad \text{equation 3}$$

1. N. G. Connelly, W. E. Geiger, *Chemical Reviews*, 1996, **96**, 877-910.